The 9th European Congress on Computational Methods in Applied Sciences and Engineering
ECCOMAS Congress 2024
3–7 June 2024, Lisboa, Portugal

# MULTIDISCIPLINARY OPTIMIZATION OF LOAD ADAPTIVE WINGS FOR HIGHLY EFFICIENT LONG-HAUL AIRLINERS

**Tobias F. Wunderlich**[1] **and Sascha Dähne**[2]

[1] German Aerospace Center, Institute of Aerodynamics and Flow Technology,
38108 Braunschweig, Lilienthalplatz 7, Germany, tobias.wunderlich@dlr.de

[2] German Aerospace Center, Institute of Lightweight Systems,
38108 Braunschweig, Lilienthalplatz 7, Germany, sascha.daehne@dlr.de

**Key words:** Multidisciplinary Design Optimization (MDO), adaptive wing, maneuver load alleviation (MLA), fiber composite, structural sizing, fluid-structure coupling

**Summary.** As part of the DLR project oLAF (optimal load-adaptive aircraft), a long-haul airliner with maneuver load alleviation limited to aileron deflections and the use of a geared turbofan engine is being designed and optimized. Adaptive wing technologies based on trailing edge control surface deflections to reduce drag at cruise and for optimal load reduction are introduced and supplemented by other structural technologies with increased strain allowable to reduce wing mass.

In this work the results of the aero-structural wing optimizations of the aircraft with advanced structural wing technologies and the aircraft with a load adaptive wing will be presented. High-fidelity simulation methods are used in the optimization process to determine the flight performance in the transonic cruise flight, the loads of the wing in maneuver flight and the mass of the wing box made of fiber composite materials. Static aeroelastic effects are considered in all flight conditions. The minimization of the fuel consumption for three typical flight missions represents the objective function. The geometric integration of the control surfaces and aircraft trimming are considered. The selected design parameters describe the twist distribution and the control surface deflections.

The consideration of structural technologies with increased strain allowable and local buckling after limit load result in a 2.9 % reduction of fuel consumption after aero-structural optimization of the twist distribution. With the introduction of adaptive wing technologies based on trailing edge control surface deflections a further fuel burn reduction between 0.8 % and 1.9 % depending on the flight mission is predicted.

## 1 INTRODUCTION

The environmental impact and resource requirements of commercial aviation are increasing with the growth of global mobility and transportation. To protect the environment and conserve resources, aviation is undergoing a transformation process toward more energy-efficient air transport. DLR's Aviation Research Strategy [1] describes and specifies the contribution of aeronautics research to achieving the goals of the mobility strategy of the European Green

Deal [2]. The corresponding target for the vehicle is a 25 % reduction in specific engine fuel consumption and a 50 % reduction in the aircraft's energy requirements.

The efficiency of commercial aircraft is determined by aerodynamic performance in terms of the lift-to-drag ratio, the empty mass of the aircraft and the thrust-specific fuel consumption of the engine. An aerodynamically optimized shape can further reduce drag in transonic cruise flight. This is achieved through advances in wing and airfoil design. Composite materials such as carbon fiber-reinforced polymers (CFRP) allow adapting the structural design to the loads by exploiting the additional degree of freedom of fiber orientation. Geared turbofan technology promises to further reduce thrust-specific fuel consumption by increasing propulsion efficiency.

In the context of aero-structural wing optimization, the optimal trade-off between cruise performance and wing mass is achieved by combining high-fidelity methods for numerical flow simulation of the aircraft outer shape and the structural sizing of the wing box with an appropriate optimization algorithm [3]. Thereby, the interaction of aerodynamic forces and wing deformations are considered to enable accurate prediction of flight performance and static maneuver loads using fluid-structure coupling.

In the design process of composite structures a damaged tolerance design allowable typically limits the permitted strain level. The dependency of the damage tolerance allowable from the ply share of the laminate has been investigated by Bogenfeld et al. [4]. Based on the results of these studies an allowable increase between 30 % and 50 % has been identified. The introduction of new structural concepts in terms of load share between skin and stiffeners (e.g. "stringer dominant design") and ply share selection an increased strain allowable results in mass reduction of the wing box. Further mass reduction potential has been identified due to permit local buckling after limit load ("post-buckling"). In addition, the increased allowables lead to more flexible wing structures that increase passive load alleviation.

Further improvements can be achieved by adapting the wing shape to the present flight condition. Adaptive wing technology has long been researched by industry and academia and has been summarized, for example, by Martins [5] under the synonym of morphing wing. For practical implementation, variable camber using trailing edge devices is the most promising type of wing morphing. The basic phenomena of variable camber, the corresponding wing design philosophy and system requirements, and the advantages of the new wing concept are described by Szodruch and Hilbig [6]. Aero-structural design optimization published by Burdette, Kenway, and Martins [7] shows a potential 1.7 % reduction in fuel consumption by using a 10 % deep continuous morphing trailing edge. Reckzeh [8] describes the wing movables concept of the Airbus A350 in service. This concept provides a functional integration of high-lift with load and cruise performance control. The potential for reducing fuel consumption by improving cruise performance has been investigated for a long-haul passenger aircraft in our own research [9]. Depending on the flight mission a fuel burn reduction between 0.5 % and 1.7 % was predicted.

## 2 METHODS

An integrated process chain for aero-structural wing optimization based on high fidelity simulation methods has been used for the presented optimizations of the twist distribution and the control surface deflections. A detailed description of the original process chain and their successful application has been published by Wunderlich et al. [3, 10]. The process chain include a mesh deformation techniques for geometry changes and simplified control surface deflections,

a landing gear integration, a tail sizing based on handbook methods and a trim drag estimation functionality. The improvements described in the current article relate to the introduction of a component based fluid structure interaction, which allows the accurate consideration of wing deformations in the presence of an engine nacelle.

### 2.1 Process for aero-structural wing optimization

The process chain applied in the present work is shown in Fig. 1 in the form of XDSM-diagrams (Extended Design Structure Matrix) [11]. In each optimization step, the aircraft description of the baseline configuration is updated according to the current values of the design parameters. The resulting aircraft description is transferred to the subsequent simulation programs using the Common Parametric Aircraft Configuration Schema (CPACS) [12].

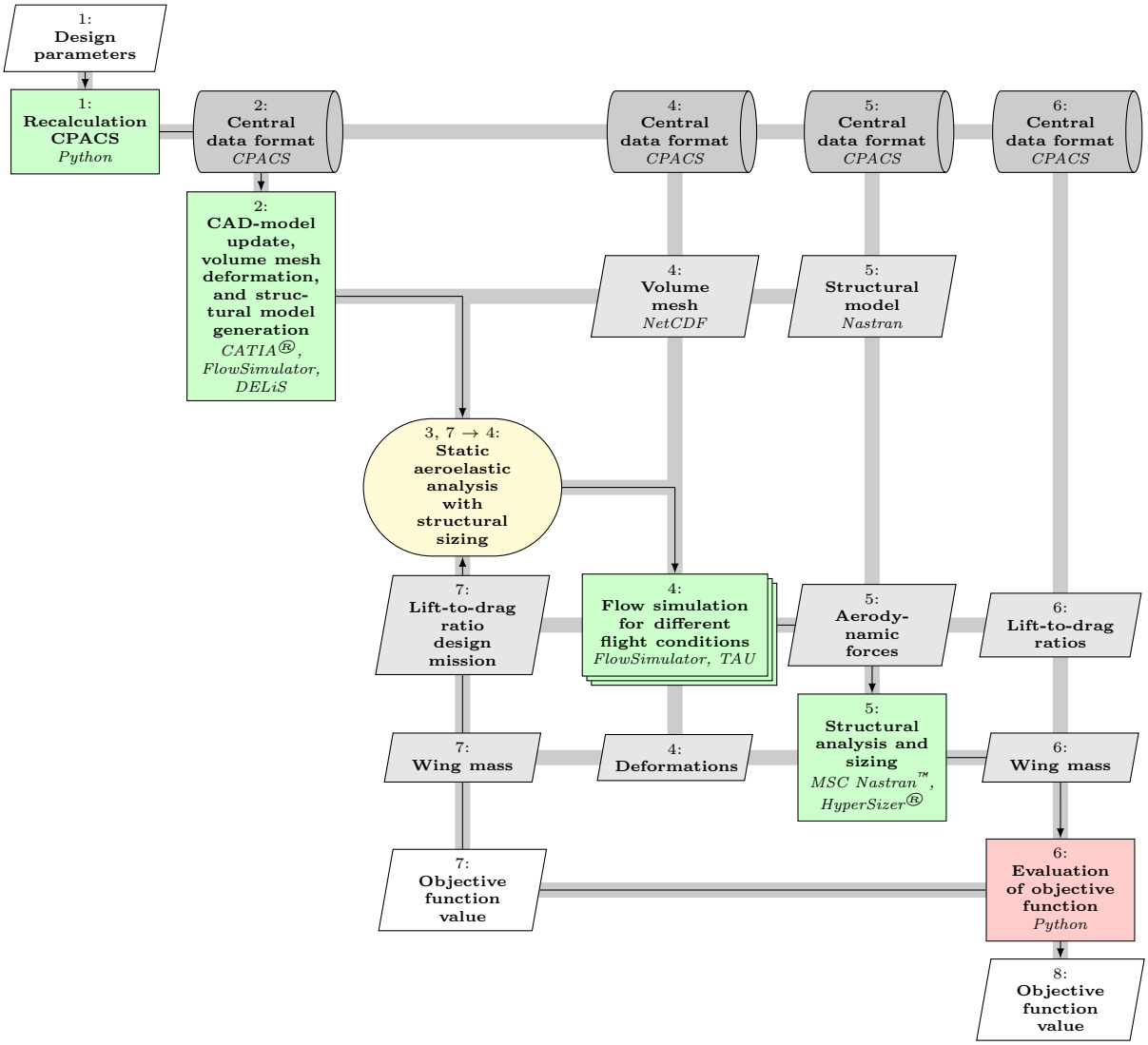


**Figure 1**: Flow chart of the process chain for aero-structural wing analysis.

In the next step the parametric CAD model is updated, the aerodynamic volume mesh is deformed, and the structural model is generated. The parametric CAD model has been built in the commercial software CATIA® V5, which enables accurate surface representation, and robust and time efficient geometry changes.

In the CFD volume mesh deformation process, the mesh representing the baseline configuration is deformed in parallel for all flight conditions. According to the control surface deflection to be generated, the displacement field of the surface mesh is computed for each flight condition. It is then transferred to the CFD volume mesh using the Elasticity Analogy (EA) mesh deformation method [13] available in the FlowSimulator [14] environment.

For the generation of the structural model the DLR in-house tool DELiS (Design Environment for thin-walled Lightweight Structures) [15] is used. Based on the central data format CPACS, DELiS automatically generates a consistent finite element mesh by using the open-source tool Gmsh [16]. The finite element model is made up of shells elements enriched with physical properties of the wing spars, ribs, and skin cells and finally exported for the commercial FE solver MSC Nastran™.

The fluid-structure coupling loop is marked with a rounded yellow box and the values of the design mission lift-to-drag ratio, the wing mass and the objective function value are evaluated for the convergence examination.

For all flight conditions the aerodynamic forces and coefficients are computed using RANS-based CFD simulations. The flow simulations are performed by using the DLR TAU-Code [17] which is integrated in the HPC framework FlowSimulator [18].

Based on the aerodynamic loads computed for the flight conditions considered, the wing-box structure is sized. Within the structural analysis and sizing process the disciplinary objective is to fulfill the structural constraints in terms of failure criteria and converge the margins of safety (MoS) and wing mass. Hence, the structural analysis and sizing process represents a subspace optimization. Different design criteria are applied to ensure a valid structural design. As proposed by Dähne et al. [19] for stiffened panels, the criteria for strength, maximum strain, and local and global buckling are used for skin and all stringer components. The main results of this process are the wing mass and the deformed wing shapes for the flight conditions considered. The structural analysis and sizing process uses the commercial software MSC Nastran™ for computing the internal loads and stresses. The commercial software HyperSizer® is applied for sizing the composite wing box.

The structural deformations form the input for the CFD volume mesh deformation. A mesh deformation method based on radial basis functions (RBF) [20] available in the FlowSimulator is used.

Afterwards, the objective function is evaluated and the convergence criteria of the static aeroelastic analysis are examined. Once convergence of the fluid-structure coupling loop is reached, the objective function value is given to the global optimizer.

## 3 DESIGN TASK

The design task describes the objective function, the design space, and the constraints. In this work the wing design for a long-haul airliner has been selected.

### 3.1 Objective function, flight missions and load cases

The objective function of the multi-mission aero-structural wing optimizations is the combined fuel consumption per range and payload of three selected flight missions. Thus, the combined fuel consumption is the weighted sum of the fuel consumption of the corresponding missions as given in Eq. (1).

$$\frac{m_F}{R\, m_P} = \sum_i w_i \left( \frac{m_F}{R\, m_P} \right)_i \tag{1}$$

Table 1 provides an overview of the selected flight missions and weighting factors. With the selected weighting factors, the expected relative frequency of the missions in airline operation has been taken into account.

| **Flight missions** | | **Study mission** | **High speed mission** | **Design mission** |
|---|---|---|---|---|
| Weighting factor | $w_i$ | 0.6 | 0.1 | 0.3 |
| Cruise Mach number | $Ma$ | 0.83 | 0.85 | 0.83 |
| Range | $R$ | 4000 nm (7408 km) | 4000 nm (7408 km) | 6000 nm (11 112 km) |
| Payload | $m_P$ | 40 800 kg | 40 800 kg | - |
| Reserve fuel ratio | $m_{F,res}/m_F$ | 0.1400 | 0.1400 | 0.1000 |
| **Flight load case** | | **Pull up maneuver** | **Push over maneuver** | **Roll maneuver** |
| Altitude | $H$ | 0 m | 3048 m | 0 m |
| Mach number | $Ma$ | 0.552 | 0.655 | 0.552 |
| Lift coefficient | $C_L$ | 0.744 | −0.305 | 0.593 |
| Load factor | $n$ | 2.5 | −1.0 | 2.0 |

**Table 1**: Flight missions and flight load cases.

For the study and design mission the design Mach number of the Airbus A330 has been selected. The design mission range is set to 6000 nm and the corresponding payload is a result of the static aeroelastic analysis. The selection of range and payload for the study mission is based on a typical long-haul mission with a passenger load factor of 0.85 and represents the mission for which the aircraft will be optimized primarily. The difference between high speed and the study mission is the increased cruise Mach number to consider off-design conditions in the wing optimization.

For the structural sizing of the wing box the maneuver load cases with the maximum loads have to be defined. These maneuver load cases have been derived from the flight envelope limits and the limits of the maneuvering load factor resulting from the certification regulations CS-25/FAR 25. In Tab. 1 an overview of the selected maneuver load cases is given. In addition to the presented maneuver flight load cases a touch down load case has been introduced to consider the landing gear loads in the wing box sizing.

A conceptual design model has been used to calculate the fuel consumption of the individual flight missions. In this model, the cruise segment of the mission is described by the well-known Breguet range equation. The thrust-specific fuel consumption has been derived from the engine map of a geared turbofan provided by the DLR-Institute of Propulsion Technology. The lift-to-drag ratio in cruise is obtained from the aerodynamic coefficients of the flow simulation for the wing-fuselage-engine configuration, the estimated aerodynamic coefficients of the tailplane and

the specified residual drag and residual thrust coefficients. The longitudinal trim of the aircraft for the given center of gravity position is taken into account. Further details on the models and equations used are described by Wunderlich et al. [3, 10].

### 3.2 Design parameters and constraints

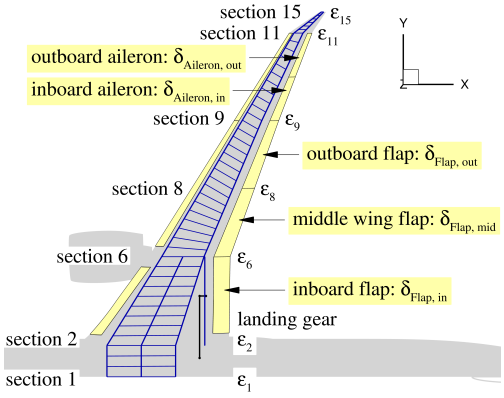


| | |
|---|---|
| Maximum take-off mass | 220 000 kg |
| Maximum payload | 54 000 kg |
| Residual mass ratio (fuselage, operating items) | 0.3952 |
| Specific mass of leading edge | 30 kg/m$^2$ |
| Specific mass of trailing edge | 50 kg/m$^2$ |
| Fuel tank volume | $V_F \geq V_{F,req}$ |
| Residual drag coefficient | 0.0018 |
| Residual thrust coefficient (through-flow nacelle) | 0.0030 |
| Center of gravity position | 36 % $c_{MAC}$ |

**Figure 2**: Design parameters and constraints.

The twist angles $\varepsilon_i$ in six wing sections and the deflection angles $\delta_j$ of five control surfaces at the trailing edge of the wing form the design parameters, as shown in Fig. 2. The wing planform, wing airfoils, and fuselage shape have been kept constant during the wing optimizations. In addition the maximum take-off mass, the maximum payload, and specific masses of the leading and trailing edges are constant. The wing mass is a result of the structural sizing of the wing box. During optimization, the required fuel tank volume is calculated for all selected flight missions and compared to the usable fuel tank volume. The aerodynamic coefficients in the aerodynamic simulation are corrected with a constant residual drag coefficient to account for drag from components that are neglected in the simulation, such as the engine pylon and flap track fairings. An additional residual thrust has been introduced to correct the coefficients in the simulation with a flow-through nacelle. Fig. 2 summarizes the constraints that have been taken into account.

### 3.3 Adaptive wing

Adaptive wing technology describes the controlled adaptation of the wing shape to different flight conditions with the aim of improving cruising performance and reducing loads in order to reduce mass and increase passenger comfort. In this work multi-functional control surfaces at the wing trailing edge have been integrated into the aircraft configuration to introduce variable camber technology. The potential of fuel burn reduction due to cruise flight performance improvement has been shown in the publication of Wunderlich and Siebert [9] for a long-haul passenger aircraft with identical top level aircraft requirements (TLARs). In comparison to this previous work, the technology of active maneuver load alleviation by the usage of trailing edge control surfaces and the structural sizing of the wing box have been added. The selection of control surfaces for cruise flight performance improvements has been derived from the results of this previous work to overcome the practical limitations in the number of design parameters.

### 3.4 Structural concept

The structural concept of the conventional composite design consists of classical wing covers ply share and T-stringers. State of the art values for the strain allowable have been selected.

For the structural concept of increased strain allowable and post-buckling, the classic skin-dominated design of the covers has been replaced by a stringer-dominated design. The selected values of the strain allowable and the corresponding percentage ply share of the covers, spars and ribs based on the calculations of damaged tolerance design allowables published by Bogenfeld et al. [4]. Furthermore, the structural technology of post-buckling has been introduced, which permits local buckling after limit load.

In Table 2 the differences between the structural concepts of the conventional composite wing design and the design with increased strain allowable and post-buckling have been summarized.

| | | **Conventional composite design** | **Increased strain allowable and post-buckling** |
|---|---|---|---|
| Structural concept of the covers | | Skin-dominated design | Stringer-dominated design |
| Stringer type | | T-stringer | T-stringer |
| Strain allowable | Tension | 4500 µm/m | 6100 µm/m |
| | Compression | 3500 µm/m | 4400 µm/m |
| | Shear | 9000 µm/m | 8800 µm/m |
| Local buckling | | No local buckling | Local buckling after limit load ("post-buckling") |
| Percentage ply share $0°/\pm 45°/90°$ | Covers center wing | 70/20/10 | 20/70/10 |
| | Covers inboard wing | 40/50/10 | 20/70/10 |
| | Covers middle wing | 40/50/10 | 20/70/10 |
| | Covers outboard wing | 30/60/10 | 20/70/10 |
| | Covers wing tip | 30/60/10 | 20/70/10 |
| | Spars | 50/40/10 | 20/70/10 |
| | Ribs | 40/50/10 | 20/70/10 |
| | Stringers | 70/20/10 | 70/20/10 |

**Table 2**: Structural concept overview.

## 4 RESULTS

The starting point for multidisciplinary wing optimization is the baseline configuration (see first column of Table 3), which is the result of a combined twist distribution and airfoil shape optimization. The wing of the baseline configuration has been optimized using state-of-the-art technology for active maneuver load reduction (MLA). The ailerons have been used with the deflection angles given in Table 3. Furthermore, the structural concept of the wing box is a conventional composite design shown in Table 2. The optimization on which the baseline configuration is based is not the subject of this publication.

Starting from the baseline configuration, the structural concept of increased strain allowable and post-buckling shown in Table 2 is introduced and a multidisciplinary wing optimization of the twist distribution is performed (see second column of Table 3). The aim of optimizing

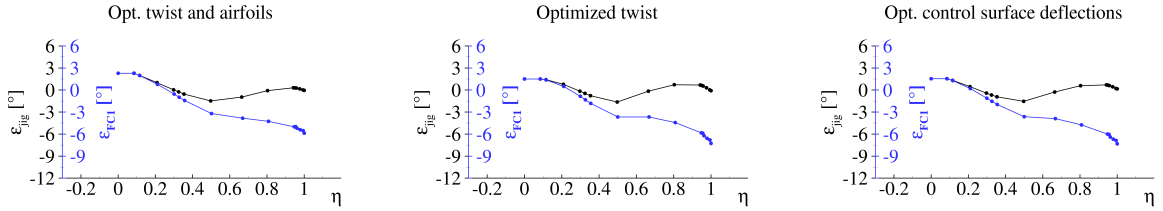


**Figure 3**: Twist distributions of baseline and optimized wings.

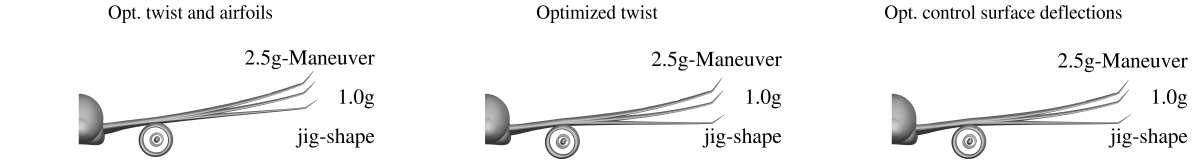


**Figure 4**: Wing deformations for cruise and maneuver flight of baseline and optimized wings.

the twist distribution is to determine the optimum lift distribution with regard to minimum fuel consumption. In addition to the flight performance in cruise flight, the structural mass of the wing resulting from the structural sizing is also taken into account, including the wing deformations. In the next wing optimization (see last column of Table 3) the adaptive wing technologies have been introduced. Thereby the control surface deflection angles and the twist distribution have been optimized together.

The corresponding results in Table 3 show an increase in the lift-to-drag ratio in all the flight missions considered and a significant reduction in the structural mass of the wing. With the introduction of adaptive wing technology, a further increase in cruise flight performance and a further reduction in wing mass has been achieved. The optimized twist distributions of the configurations with advanced structural and adaptive wing technologies in Figure 4 show greater differences between the twist angles in the unloaded state ("jig shape") in black compared to cruise flight in blue due to the increase in wing deformations shown in Figure 4.

It should also be noted that the wings with the structural concept of increased strain allowable and post-buckling have a reduced dihedral compared to the baseline configuration in order to counteract the loss of lift due to the wing deformations in the outer wing region.

Figure 6 presents the lift force and lift coefficient distributions for the baseline configuration and the optimized configurations with advanced structural and adaptive wing technologies. The corresponding center of lift is shown as a black circle and the value is given in Table 3. For each lift distribution, the related elliptical lift distribution is shown by a dashed line, and the corresponding center of lift is indicated by a gray square. The elliptical lift distribution is the optimum for planar wings in terms of lift induced drag. The increase in the lift-to-drag ratio in cruise flight can be explained by the more favorable lift distribution with regard to the induced drag. This outboard shift of lift is aerodynamically limited by an increase in the local lift coefficient (blue line in Figure 6) at the outer wing and the corresponding non-linear increase in transonic wave drag.

| | | **Opt. twist and airfoils (Baseline)** | **Opt. twist** | **Opt. control surface deflections** |
|---|---|---|---|---|
| **Structural concept** | | conventional | increased strain allowable and post-buckling | increased strain allowable and post-buckling |
| **Masses** | | | | |
| Mass of covers | $m_{W,covers}$ | 6734 kg | 5969 kg | 5958 kg |
| Mass of spars | $m_{W,spars}$ | 2306 kg | 1987 kg | 1958 kg |
| Mass of ribs | $m_{W,ribs}$ | 1686 kg | 1565 kg | 1598 kg |
| Wing box mass[a] | $m_{W,box}$ | 13 408 kg | 11 900 kg | 11 892 kg |
| Wing mass ratio | $m_W/m_{MTO}$ | 0.0996 | 0.0928 | 0.0928 |
| Operational empty mass ratio | $m_{OE}/m_{MTO}$ | 0.5115 | 0.5047 | 0.5047 |
| **Maneuver n=2.5** | | | | |
| Control surface deflections | $\delta_{Flap,\,in}$ | 0.0° | 0.0° | +11.0° |
| | $\delta_{Aileron,\,in}$ | −10.0° | −10.0° | −4.6° |
| | $\delta_{Aileron,\,out}$ | −15.0° | −15.0° | −13.5° |
| Center of pressure | $y_{CoP}/(b/2)$ | 0.3386 | 0.3386 | 0.3221 |
| **Maneuver n=-1.0** | | | | |
| Control surface deflections | $\delta_{Flap,\,in}$ | 0.0° | 0.0° | −12.1° |
| | $\delta_{Aileron,\,in}$ | +5.0° | +5.0° | +16.0° |
| | $\delta_{Aileron,\,out}$ | +10.0° | +10.0° | +6.7° |
| Center of pressure | $y_{CoP}/(b/2)$ | 0.3419 | 0.3292 | 0.2476 |
| **Study mission** | | | | |
| Control surface deflections | $\delta_{Flap,\,in}$ | 0.0° | 0.0° | −2.0° |
| Lift-to-drag ratio | $L/D$ | 18.20 | 18.32 | 18.50 |
| Center of pressure | $y_{CoP}/(b/2)$ | 0.3777 | 0.3804 | 0.3895 |
| Fuel consumption | $m_F/(R\,m_P)$ | $1.4056 \times 10^{-4}\,\mathrm{km}^{-1}$ | $1.3819 \times 10^{-4}\,\mathrm{km}^{-1}$ | $1.3681 \times 10^{-4}\,\mathrm{km}^{-1}$ |
| **High speed mission** | | | | |
| Control surface deflections | $\delta_{Flap,\,in}$ | 0.0° | 0.0° | −1.9° |
| | $\delta_{Flap,\,mid}$ | 0.0° | 0.0° | −1.8° |
| | $\delta_{Flap,\,out}$ | 0.0° | 0.0° | −1.1° |
| Lift-to-drag ratio | $L/D$ | 17.23 | 17.37 | 17.51 |
| Center of pressure | $y_{CoP}/(b/2)$ | 0.3764 | 0.3790 | 0.3852 |
| Fuel consumption | $m_F/(R\,m_P)$ | $1.4735 \times 10^{-4}\,\mathrm{km}^{-1}$ | $1.4473 \times 10^{-4}\,\mathrm{km}^{-1}$ | $1.4351 \times 10^{-4}\,\mathrm{km}^{-1}$ |
| **Design mission** | | | | |
| Control surface deflections | $\delta_{Flap,\,in}$ | 0.0° | 0.0° | −1.7° |
| Payload | $m_P$ | 36 597 kg | 38 479 kg | 38 961 kg |
| Used fuel tank volume ratio | $V_{F,req}/V_F$ | 0.9010 | 0.8946 | 0.8887 |
| Lift-to-drag ratio | $L/D$ | 18.31 | 18.45 | 18.61 |
| Center of pressure | $y_{CoP}/(b/2)$ | 0.3758 | 0.3781 | 0.3856 |
| Fuel consumption | $m_F/(R\,m_P)$ | $1.5845 \times 10^{-4}\,\mathrm{km}^{-1}$ | $1.4986 \times 10^{-4}\,\mathrm{km}^{-1}$ | $1.4702 \times 10^{-4}\,\mathrm{km}^{-1}$ |
| **Objective** | | | | |
| Combined fuel consumption | $m_F/(R\,m_P)$ | $1.4661 \times 10^{-4}\,\mathrm{km}^{-1}$ | $1.4234 \times 10^{-4}\,\mathrm{km}^{-1}$ | $1.4054 \times 10^{-4}\,\mathrm{km}^{-1}$ |
| $CO_2$ emissions per passenger kilometres[b] | $m_{CO2}/(R\,m_P)$ | 48.5 $g_{CO2}$/pkm | 47.1 $g_{CO2}$/pkm | 46.5 $g_{CO2}$/pkm |

[a] Values are scaled by a factor of 1.25 to account for additional masses of local reinforcements and fasteners.
[b] Values of 3.15 $kg_{CO2}/kg_{Fuel}$ for a turbofan engine [21] and 105 kg for the passenger mass with baggage are assumed.

**Table 3**: Results overview of wing optimizations.

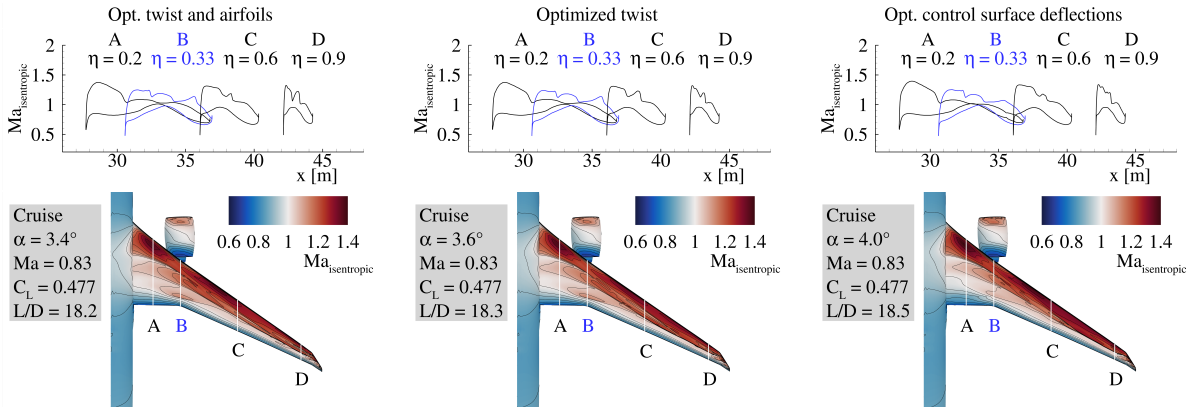


**Figure 5**: Isentropic Mach number distributions for cruise flight of baseline and optimized wings.

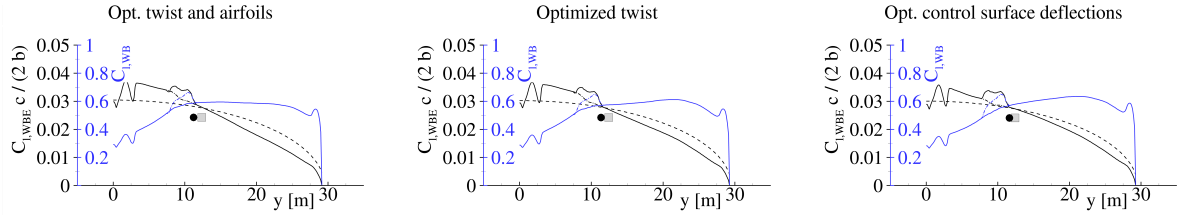


**Figure 6**: Lift and lift coefficient distributions for cruise flight of baseline and optimized wings.

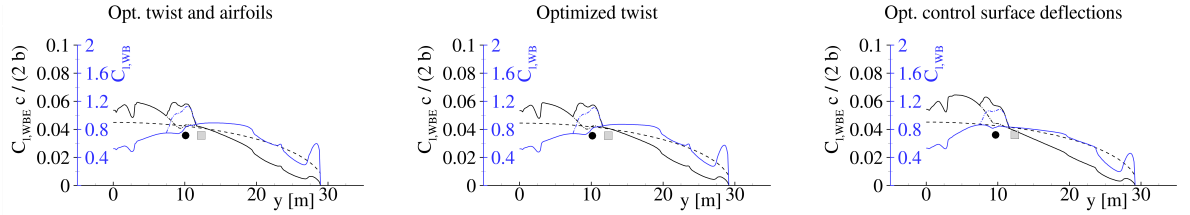


**Figure 7**: Lift and lift coefficient distributions for maneuver flight of baseline and optimized wings.

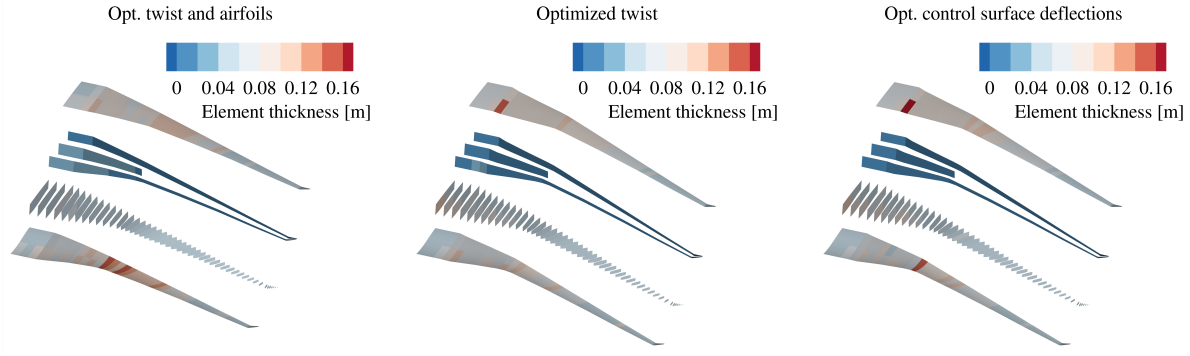


**Figure 8**: Wing box element thickness (skin thickness + stringer height) distributions of baseline and optimized wings.

Figure 5 presents the isentropic Mach number distributions of the baseline configuration and the optimized configurations with structural and adaptive wing technologies for the study mission. This figure shows the effect of the outboard shift of lift as a result of the optimized twist distribution for the advanced wing structure. Here, the outboard shift of lift leads to more pronounced compression shocks in the middle wing region, resulting in an increase in wave drag. The optimized adaptive wing uses the control surface deflections for further adaptation of the lift distribution to the current flight condition. The improvements in cruise performance in terms of lift-to-drag ratio result from the optimum compromise between induced and transonic wave drag.

Figure 7 shows the lift distributions for the maneuver with a load factor of $n = 2.5$, which is decisive for the structural sizing. Here, the pronounced shift of the lift towards the inner wing becomes clear. This shift significantly reduces the aerodynamic loads and is due to the aeroelastic effects of the swept-back wing and the control surface deflections for load reduction. With the introduction of the load-adaptive wing, the inner flap is also included for active maneuver load reduction. In contrast to the fixed aileron deflections, the adaptive wing optimizes the control surface deflections. The resulting element thickness distributions are shown in Figure 8 for the baseline configuration and the optimized configurations with structural and adaptive wing technologies. In Table 3 the corresponding mass breakdown of the wing box is given. With the introduction of the advanced structural concept, a significant reduction in the primary wing mass in the order of 600 kg has been achieved.

## 5 CONCLUSION AND OUTLOOK

In this work, the assessment of the structural concept with increased strain allowable and the adaptive wing technology have been successfully demonstrated by using an integrated process for aero-structural wing optimization based on high fidelity simulation methods. The comparison of optimization results with the same objective function, and constraints allows a proper technology assessment.

In order to find the optimum trade-off between aerodynamic performance and wing mass for the advanced structural concept, the twist distribution of the wing has been optimized. The results of this optimization show the expected reduction of the combined fuel consumption due to a reduced wing mass and increased aerodynamic performance under cruise flight conditions. With the application of this structural concept the flexibility of the wings increases and the significance of static aeroelastic effects for the prediction of cruise flight performance and passive maneuver load alleviation has been shown.

Based on lift distributions designed for an optimal trade-off between lift-to-drag ratio and structural mass, adapting the lift distribution to the current flight condition enables improvements in cruise performance without drawbacks in structural mass. This increase in aerodynamic performance has been achieved by finding the optimal compromise between induced and transonic wave drag. The adaptation of the wing shape to the current deformation due to mass changes during the flight mission becomes more important as the flexibility of the wing increases.

In the future, adaptation of lift distribution for optimum cruise performance and maneuver load alleviation have to be considered in aero-structural airfoil shape and wing planform optimization.

## References


[1] German Aerospace Center. *Towards zero-emission Aviation - How DLR's Aviation Research Strategy supports the European Green Deal 2050.* Cologne, Germany: German Aerospace Center (DLR), 2022.

[2] European Commision. *Sustainable and Smart Mobility Strategy.* Luxembourg, Belgium: Office for Official Publications of the European Communities, Dec. 2020.

[3] T. F. Wunderlich et al. "Global Aerostructural Design Optimization of More Flexible Wings for Commercial Aircraft". In: *Journal of Aircraft* 58.6 (2021), pp. 1254–1271.

[4] R. M. Bogenfeld et al. "Damage Tolerance Allowable Calculation for the Aircraft Design with Static Ultimate Load". In: *Composite Structures* (Dec. 2023). Ed. by N. Fantuzzi et al.

[5] J. R. R. A. Martins. "Fuel Burn Reduction Through Wing Morphing". In: *Encyclopedia of Aerospace Engineering.* John Wiley & Sons, Ltd, 2016, pp. 1–7.

[6] J. Szodruch and R. Hilbig. "Variable wing camber for transport aircraft". In: *Progress in Aerospace Sciences* 25.3 (1988), pp. 297–328.

[7] D. A. Burdette et al. "Aerostructural design optimization of a continuous morphing trailing edge aircraft for improved mission performance". In: *17th AIAA/ISSMO Multidisciplinary Analysis and Optimization Conference.*

[8] D. Reckzeh. "Multifunctional Wing Moveables: Design of the A350XWB and the Way to Future Concepts". In: *29th Congress of the International Council of the Aeronautical Sciences, ICAS 2014.* Sept. 2014.

[9] T. F. Wunderlich and F. Siebert. "Optimization of control surface deflections on the high aspect ratio wing to improve cruise flight performance". In: *New Results in Numerical and Experimental Fluid Mechanics XIV- Contributions to the 23rd STAB/DGLR Symposium Berlin.* Ed. by A. Dillmann et al. Cham: Springer, Nov. 2022, pp. 206–215.

[10] T. F. Wunderlich and L. Reimer. "Integrated Process Chain for Aerostructural Wing Optimization and Application to an NLF Forward Swept Composite Wing". In: *AeroStruct: Enable and Learn How to Integrate Flexibility in Design.* Ed. by R. Heinrich. Vol. 138. Notes on Numerical Fluid Mechanics and Multidisciplinary Design (NNFM). Cham: Springer International Publishing, 2018, pp. 3–33.

[11] A. B. Lambe and J. R. R. A. Martins. "Extensions to the Design Structure Matrix for the Description of Multidisciplinary Design Analysis and Optimization Processes". In: *Structural and Multidisciplinary Optimization* 46 (2012), pp. 273–284.

[12] C. M. Liersch and M. Hepperle. "A distributed toolbox for multidisciplinary preliminary aircraft design". In: *CEAS Aeronautical Journal* 2.1–4 (2011), pp. 57–68.

[13] A. Rempke. "Netzdeformation mit Elastizitätsanalogie in multidisziplinärer FlowSimulator-Umgebung". In: *20. DGLR - Fach - Symposium der STAB 2016.* Vol. 2016. 2016, pp. 128–129.

[14] L. Reimer et al. "Towards Higher-Precision Maneuver and Gust Loads Computations of Aircraft: Status of Related Features in the CFD-Based Multidisciplinary Simulation Environment FlowSimulator". In: *New Results in Numerical and Experimental Fluid Mechanics XII.* Ed. by A. Dillmann et al. Cham: Springer International Publishing, 2020, pp. 597–607.

[15] T. Führer et al. “Automated model generation and sizing of aircraft structures”. In: *Aircraft Engineering and Aerospace Technology* 88.2 (2016), pp. 268–276.

[16] C. Geuzaine and J.-F. Remacle. “Gmsh: A 3-D finite element mesh generator with built-in pre- and post-processing facilities”. In: *International Journal for Numerical Methods in Engineering* 79.11 (2009), pp. 1309–1331.

[17] T. Gerhold. “Overview of the Hybrid RANS TAU-Code”. In: *MEGAFLOW - Numerical Flow Simulation for Aircraft Design*. Ed. by N. Kroll and J. K. Fassbender. Vol. 89. Berlin, Heidelberg: Springer Berlin Heidelberg, 2005, pp. 81–92.

[18] M. Meinel and G. O. Einarsson. “The FlowSimulator framework for massively parallel CFD applications”. In: *PARA 2010 conference, 6-9 June, Reykjavik, Iceland*. 2010.

[19] S. Dähne et al. “Steps to Feasibility for Laminar Wing Design in a Multidisciplinary Environment”. In: *29th Congress of the International Council of the Aeronautical Sciences, ICAS 2014*. Sept. 2014.

[20] H. Barnewitz and B. Stickan. “Improved Mesh Deformation”. In: *Management and Minimisation of Uncertainties and Errors in Numerical Aerodynamics: Results of the German collaborative project MUNA*. Ed. by B. Eisfeld et al. Vol. 122. Berlin, Heidelberg, 2013, pp. 219–243.

[21] N. E. Antoine and I. M. Kroo. “Aircraft Optimization for Minimal Environmental Impact”. In: *Journal of Aircraft* 41.4 (2004), pp. 790–797.